EUROPEAN ORGANIZATION FOR NUCLEAR RESEARCH

Measurement of Inclusive ρ^0, $f_0(980)$, $f_2(1270)$, $K_2^{*0}(1430)$ and $f_2'(1525)$ Production in Z^0 Decays

DELPHI Collaboration

Abstract

DELPHI results are presented on the inclusive production of the neutral mesons ρ^0, $f_0(980)$, $f_2(1270)$, $K_2^{*0}(1430)$ and $f_2'(1525)$ in hadronic Z^0 decays. They are based on about 2 million multihadronic events collected in 1994 and 1995, using the particle identification capabilities of the DELPHI Ring Imaging Cherenkov detectors and measured ionization losses in the Time Projection Chamber. The total production rates per hadronic Z^0 decay have been determined to be: 1.19 ± 0.10 for ρ^0; 0.164 ± 0.021 for $f_0(980)$; 0.214 ± 0.038 for $f_2(1270)$; 0.073 ± 0.023 for $K_2^{*0}(1430)$; and 0.012 ± 0.006 for $f_2'(1525)$. The total production rates for all mesons and differential cross-sections for the ρ^0, $f_0(980)$ and $f_2(1270)$ are compared with the results of other LEP experiments and with models.

P.Abreu[21], W.Adam[50], T.Adye[36], P.Adzic[11], I.Ajinenko[42], Z.Albrecht[17], T.Alderweireld[2], G.D.Alekseev[16], R.Alemany[49], T.Allmendinger[17], P.P.Allport[22], S.Almehed[24], U.Amaldi[9], S.Amato[47], E.G.Anassontzis[3], P.Andersson[44], A.Andreazza[9], S.Andringa[21], P.Antilogus[25], W-D.Apel[17], Y.Arnoud[9], B.Åsman[44], J-E.Augustin[25], A.Augustinus[9], P.Baillon[9], P.Bambade[19], F.Barao[21], G.Barbiellini[46], R.Barbier[25], D.Y.Bardin[16], G.Barker[9], A.Baroncelli[38], M.Battaglia[15], M.Baubillier[23], K-H.Becks[52], M.Begalli[6], P.Beilliere[8], Yu.Belokopytov[9,53], A.C.Benvenuti[5], C.Berat[14], M.Berggren[25], D.Bertini[25], D.Bertrand[2], M.Besancon[39], F.Bianchi[45], M.Bigi[45], M.S.Bilenky[16], M-A.Bizouard[19], D.Bloch[10], H.M.Blom[30], M.Bonesini[27], W.Bonivento[27], M.Boonekamp[39], P.S.L.Booth[22], A.W.Borgland[4], G.Borisov[19], C.Bosio[41], O.Botner[48], E.Boudinov[30], B.Bouquet[19], C.Bourdarios[19], T.J.V.Bowcock[22], I.Boyko[16], I.Bozovic[11], M.Bozzo[13], P.Branchini[38], T.Brenke[52], R.A.Brenner[48], P.Bruckman[18], J-M.Brunet[8], L.Bugge[32], T.Buran[32], T.Burgsmueller[52], P.Buschmann[52], S.Cabrera[49], M.Caccia[27], M.Calvi[27], T.Camporesi[9], V.Canale[37], F.Carena[9], L.Carroll[22], C.Caso[13], M.V.Castillo Gimenez[49], A.Cattai[9], F.R.Cavallo[5], V.Chabaud[9], Ph.Charpentier[9], L.Chaussard[25], P.Checchia[35], G.A.Chelkov[16], R.Chierici[45], P.Chliapnikov[42], P.Chochula[7], V.Chorowicz[25], J.Chudoba[29], K.Cieslik[18], P.Collins[9], R.Contri[13], E.Cortina[49], G.Cosme[19], F.Cossutti[9], J-H.Cowell[22], H.B.Crawley[1], D.Crennell[36], S.Crepe[14], G.Crosetti[13], J.Cuevas Maestro[33], S.Czellar[15], G.Damgaard[28], M.Davenport[9], W.Da Silva[23], A.Deghorain[2], G.Della Ricca[46], P.Delpierre[26], N.Demaria[9], A.De Angelis[9], W.De Boer[17], S.De Brabandere[2], C.De Clercq[2], B.De Lotto[46], A.De Min[35], L.De Paula[47], H.Dijkstra[9], L.Di Ciaccio[37], J.Dolbeau[8], K.Doroba[51], M.Dracos[10], J.Drees[52], M.Dris[31], A.Duperrin[25], J-D.Durand[9], G.Eigen[4], T.Ekelof[48], G.Ekspong[44], M.Ellert[48], M.Elsing[9], J-P.Engel[10], B.Erzen[43], M.Espirito Santo[21], E.Falk[24], G.Fanourakis[11], D.Fassouliotis[11], J.Fayot[23], M.Feindt[17], P.Ferrari[27], A.Ferrer[49], E.Ferrer-Ribas[19], S.Fichet[23], A.Firestone[1], U.Flagmeyer[52], H.Foeth[9], E.Fokitis[31], F.Fontanelli[13], B.Franek[36], A.G.Frodesen[4], F.Fulda-Quenzer[19], J.Fuster[49], A.Galloni[22], D.Gamba[45], S.Gamblin[19], M.Gandelman[47], C.Garcia[49], C.Gaspar[9], M.Gaspar[47], U.Gasparini[35], Ph.Gavillet[9], E.N.Gazis[31], D.Gele[10], L.Gerdyukov[42], N.Ghodbane[25], I.Gil[49], F.Glege[52], R.Gokieli[9,51], B.Golob[43], G.Gomez-Ceballos[40], P.Goncalves[21], I.Gonzalez Caballero[40], G.Gopal[36], L.Gorn[1,54], M.Gorski[51], Yu.Gouz[42], V.Gracco[13], J.Grahl[1], E.Graziani[38], C.Green[22], H-J.Grimm[17], P.Gris[39], G.Grosdidier[19], K.Grzelak[51], M.Gunther[48], J.Guy[36], F.Hahn[9], S.Hahn[52], S.Haider[9], A.Hallgren[48], K.Hamacher[52], J.Hansen[32], F.J.Harris[34], V.Hedberg[24], S.Heising[17], J.J.Hernandez[49], P.Herquet[2], H.Herr[9], T.L.Hessing[34], J.-M.Heuser[52], E.Higon[49], S-O.Holmgren[44], P.J.Holt[34], S.Hoorelbeke[2], M.Houlden[22], J.Hrubec[50], K.Huet[2], G.J.Hughes[22], K.Hultqvist[44], J.N.Jackson[22], R.Jacobsson[9], P.Jalocha[9], R.Janik[7], Ch.Jarlskog[24], G.Jarlskog[24], P.Jarry[39], B.Jean-Marie[19], E.K.Johansson[44], P.Jonsson[25], C.Joram[9], P.Juillot[10], F.Kapusta[23], K.Karafasoulis[11], S.Katsanevas[25], E.C.Katsoufis[31], R.Keranen[17], B.P.Kersevan[43], B.A.Khomenko[16], N.N.Khovanski[16], A.Kiiskinen[15], B.King[22], A.Kinvig[22], N.J.Kjaer[30], O.Klapp[52], H.Klein[9], P.Kluit[30], P.Kokkinias[11], M.Koratzinos[9], V.Kostioukhine[42], C.Kourkoumelis[3], O.Kouznetsov[16], M.Krammer[50], E.Kriznic[43], J.Krstic[11], Z.Krumstein[16], P.Kubinec[7], J.Kurowska[51], K.Kurvinen[15], J.W.Lamsa[1], D.W.Lane[1], P.Langefeld[52], V.Lapin[42], J-P.Laugier[39], R.Lauhakangas[15], G.Leder[50], F.Ledroit[14], V.Lefebure[2], L.Leinonen[44], A.Leisos[11], R.Leitner[29], G.Lenzen[52], V.Lepeltier[19], T.Lesiak[18], M.Lethuillier[39], J.Libby[34], D.Liko[9], A.Lipniacka[44], I.Lippi[35], B.Loerstad[24], J.G.Loken[34], J.H.Lopes[47], J.M.Lopez[40], R.Lopez-Fernandez[14], D.Loukas[11], P.Lutz[39], L.Lyons[34], J.MacNaughton[50], J.R.Mahon[6], A.Maio[21], A.Malek[52], T.G.M.Malmgren[44], V.Malychev[16], F.Mandl[50], J.Marco[40], R.Marco[40], B.Marechal[47], M.Margoni[35], J-C.Marin[9], C.Mariotti[9], A.Markou[11], C.Martinez-Rivero[19], F.Martinez-Vidal[49], S.Marti i Garcia[9], J.Masik[12], N.Mastroyiannopoulos[11], F.Matorras[40], C.Matteuzzi[27], G.Matthiae[37], F.Mazzucato[35], M.Mazzucato[35], M.Mc Cubbin[22], R.Mc Kay[1], R.Mc Nulty[22], G.Mc Pherson[22], C.Meroni[27], W.T.Meyer[1], A.Miagkov[42], E.Migliore[45], L.Mirabito[25], W.A.Mitaroff[50], U.Mjoernmark[24], T.Moa[44], M.Moch[17], R.Moeller[28], K.Moenig[9], M.R.Monge[13], X.Moreau[23], P.Morettini[13], G.Morton[34], U.Mueller[52], K.Muenich[52], M.Mulders[30], C.Mulet-Marquis[14], R.Muresan[24], W.J.Murray[36], B.Muryn[14,18], G.Myatt[34], T.Myklebust[32], F.Naraghi[14], F.L.Navarria[5], S.Navas[49], K.Nawrocki[51], P.Negri[27], N.Neufeld[9], N.Neumeister[50], R.Nicolaidou[14], B.S.Nielsen[28], M.Nikolenko[10,16], V.Nomokonov[15], A.Normand[22], A.Nygren[24], V.Obraztsov[42], A.G.Olshevski[16], A.Onofre[21], R.Orava[15], G.Orazi[10], K.Osterberg[15], A.Ouraou[39], M.Paganoni[27], S.Paiano[5], R.Pain[23], R.Paiva[21], J.Palacios[34], H.Palka[18], Th.D.Papadopoulou[31], K.Papageorgiou[11], L.Pape[9], C.Parkes[9], F.Parodi[13], U.Parzefall[22], A.Passeri[38], O.Passon[52], M.Pegoraro[35], L.Peralta[21], M.Pernicka[50], A.Perrotta[5], C.Petridou[46], A.Petrolini[13], H.T.Phillips[36], F.Pierre[39], M.Pimenta[21], E.Piotto[27], T.Podobnik[43], M.E.Pol[6], G.Polok[18], P.Poropat[46], V.Pozdniakov[16], P.Privitera[37], N.Pukhaeva[16], A.Pullia[27], D.Radojicic[34], S.Ragazzi[27], H.Rahmani[31], D.Rakoczy[50], P.N.Ratoff[20], A.L.Read[32], P.Rebecchi[9], N.G.Redaelli[27], M.Regler[50], D.Reid[30], R.Reinhardt[52], P.B.Renton[34], L.K.Resvanis[3], F.Richard[19], J.Ridky[12], G.Rinaudo[45], O.Rohne[32], A.Romero[45], P.Ronchese[35], E.I.Rosenberg[1], P.Rosinsky[7], P.Roudeau[19], T.Rovelli[5], Ch.Royon[39], V.Ruhlmann-Kleider[39], A.Ruiz[40], H.Saarikko[15], Y.Sacquin[39], A.Sadovsky[16], G.Sajot[14], J.Salt[49], D.Sampsonidis[11], M.Sannino[13], H.Schneider[17], Ph.Schwemling[23], U.Schwickerath[17], M.A.E.Schyns[52], F.Scuri[46], P.Seager[20], Y.Sedykh[16], A.M.Segar[34], R.Sekulin[36], R.C.Shellard[6], A.Sheridan[22], M.Siebel[52], L.Simard[39], F.Simonetto[35], A.N.Sisakian[16], G.Smadja[25], O.Smirnova[24], G.R.Smith[36], A.Sokolov[42], A.Sopczak[17], R.Sosnowski[51], T.Spassov[21], E.Spiriti[38], P.Sponholz[52], S.Squarcia[13], D.Stampfer[50], C.Stanescu[38], S.Stanic[43], K.Stevenson[34], A.Stocchi[19], J.Strauss[50], R.Strub[10], B.Stugu[4], M.Szczekowski[51], M.Szeptycka[51], T.Tabarelli[27], O.Tchikilev[42], F.Tegenfeldt[48], F.Terranova[27], J.Thomas[34], J.Timmermans[30], N.Tinti[5], L.G.Tkatchev[16], S.Todorova[10], A.Tomaradze[2], B.Tome[21], A.Tonazzo[9], L.Tortora[38],

G.Transtromer[24], D.Treille[9], G.Tristram[8], M.Trochimczuk[51], C.Troncon[27], A.Tsirou[9], M-L.Turluer[39], I.A.Tyapkin[16], S.Tzamarias[11], B.Ueberschaer[52], O.Ullaland[9], V.Uvarov[42], G.Valenti[5], E.Vallazza[46], G.W.Van Apeldoorn[30], P.Van Dam[30], W.K.Van Doninck[2], J.Van Eldik[30], A.Van Lysebetten[2], I.Van Vulpen[30], N.Vassilopoulos[34], G.Vegni[27], L.Ventura[35], W.Venus[36,9], F.Verbeure[2], M.Verlato[35], L.S.Vertogradov[16], V.Verzi[37], D.Vilanova[39], L.Vitale[46], E.Vlasov[42], A.S.Vodopyanov[16], C.Vollmer[17], G.Voulgaris[3], V.Vrba[12], H.Wahlen[52], C.Walck[44], C.Weiser[17], D.Wicke[52], J.H.Wickens[2], G.R.Wilkinson[9], M.Winter[10], M.Witek[18], G.Wolf[9], J.Yi[1], O.Yushchenko[42], A.Zalewska[18], P.Zalewski[51], D.Zavrtanik[43], E.Zevgolatakos[11], N.I.Zimin[16,24], G.C.Zucchelli[44], G.Zumerle[35]

[1] Department of Physics and Astronomy, Iowa State University, Ames IA 50011-3160, USA
[2] Physics Department, Univ. Instelling Antwerpen, Universiteitsplein 1, BE-2610 Wilrijk, Belgium
  and IIHE, ULB-VUB, Pleinlaan 2, BE-1050 Brussels, Belgium
  and Faculté des Sciences, Univ. de l'Etat Mons, Av. Maistriau 19, BE-7000 Mons, Belgium
[3] Physics Laboratory, University of Athens, Solonos Str. 104, GR-10680 Athens, Greece
[4] Department of Physics, University of Bergen, Allégaten 55, NO-5007 Bergen, Norway
[5] Dipartimento di Fisica, Università di Bologna and INFN, Via Irnerio 46, IT-40126 Bologna, Italy
[6] Centro Brasileiro de Pesquisas Físicas, rua Xavier Sigaud 150, BR-22290 Rio de Janeiro, Brazil
  and Depto. de Física, Pont. Univ. Católica, C.P. 38071 BR-22453 Rio de Janeiro, Brazil
  and Inst. de Física, Univ. Estadual do Rio de Janeiro, rua São Francisco Xavier 524, Rio de Janeiro, Brazil
[7] Comenius University, Faculty of Mathematics and Physics, Mlynska Dolina, SK-84215 Bratislava, Slovakia
[8] Collège de France, Lab. de Physique Corpusculaire, IN2P3-CNRS, FR-75231 Paris Cedex 05, France
[9] CERN, CH-1211 Geneva 23, Switzerland
[10] Institut de Recherches Subatomiques, IN2P3 - CNRS/ULP - BP20, FR-67037 Strasbourg Cedex, France
[11] Institute of Nuclear Physics, N.C.S.R. Demokritos, P.O. Box 60228, GR-15310 Athens, Greece
[12] FZU, Inst. of Phys. of the C.A.S. High Energy Physics Division, Na Slovance 2, CZ-180 40, Praha 8, Czech Republic
[13] Dipartimento di Fisica, Università di Genova and INFN, Via Dodecaneso 33, IT-16146 Genova, Italy
[14] Institut des Sciences Nucléaires, IN2P3-CNRS, Université de Grenoble 1, FR-38026 Grenoble Cedex, France
[15] Helsinki Institute of Physics, HIP, P.O. Box 9, FI-00014 Helsinki, Finland
[16] Joint Institute for Nuclear Research, Dubna, Head Post Office, P.O. Box 79, RU-101 000 Moscow, Russian Federation
[17] Institut für Experimentelle Kernphysik, Universität Karlsruhe, Postfach 6980, DE-76128 Karlsruhe, Germany
[18] Institute of Nuclear Physics and University of Mining and Metalurgy, Ul. Kawiory 26a, PL-30055 Krakow, Poland
[19] Université de Paris-Sud, Lab. de l'Accélérateur Linéaire, IN2P3-CNRS, Bât. 200, FR-91405 Orsay Cedex, France
[20] School of Physics and Chemistry, University of Lancaster, Lancaster LA1 4YB, UK
[21] LIP, IST, FCUL - Av. Elias Garcia, 14-1°, PT-1000 Lisboa Codex, Portugal
[22] Department of Physics, University of Liverpool, P.O. Box 147, Liverpool L69 3BX, UK
[23] LPNHE, IN2P3-CNRS, Univ. Paris VI et VII, Tour 33 (RdC), 4 place Jussieu, FR-75252 Paris Cedex 05, France
[24] Department of Physics, University of Lund, Sölvegatan 14, SE-223 63 Lund, Sweden
[25] Université Claude Bernard de Lyon, IPNL, IN2P3-CNRS, FR-69622 Villeurbanne Cedex, France
[26] Univ. d'Aix - Marseille II - CPP, IN2P3-CNRS, FR-13288 Marseille Cedex 09, France
[27] Dipartimento di Fisica, Università di Milano and INFN, Via Celoria 16, IT-20133 Milan, Italy
[28] Niels Bohr Institute, Blegdamsvej 17, DK-2100 Copenhagen Ø, Denmark
[29] NC, Nuclear Centre of MFF, Charles University, Areal MFF, V Holesovickach 2, CZ-180 00, Praha 8, Czech Republic
[30] NIKHEF, Postbus 41882, NL-1009 DB Amsterdam, The Netherlands
[31] National Technical University, Physics Department, Zografou Campus, GR-15773 Athens, Greece
[32] Physics Department, University of Oslo, Blindern, NO-1000 Oslo 3, Norway
[33] Dpto. Fisica, Univ. Oviedo, Avda. Calvo Sotelo s/n, ES-33007 Oviedo, Spain
[34] Department of Physics, University of Oxford, Keble Road, Oxford OX1 3RH, UK
[35] Dipartimento di Fisica, Università di Padova and INFN, Via Marzolo 8, IT-35131 Padua, Italy
[36] Rutherford Appleton Laboratory, Chilton, Didcot OX11 OQX, UK
[37] Dipartimento di Fisica, Università di Roma II and INFN, Tor Vergata, IT-00173 Rome, Italy
[38] Dipartimento di Fisica, Università di Roma III and INFN, Via della Vasca Navale 84, IT-00146 Rome, Italy
[39] DAPNIA/Service de Physique des Particules, CEA-Saclay, FR-91191 Gif-sur-Yvette Cedex, France
[40] Instituto de Fisica de Cantabria (CSIC-UC), Avda. los Castros s/n, ES-39006 Santander, Spain
[41] Dipartimento di Fisica, Università degli Studi di Roma La Sapienza, Piazzale Aldo Moro 2, IT-00185 Rome, Italy
[42] Inst. for High Energy Physics, Serpukov P.O. Box 35, Protvino, (Moscow Region), Russian Federation
[43] J. Stefan Institute, Jamova 39, SI-1000 Ljubljana, Slovenia and Laboratory for Astroparticle Physics,
  Nova Gorica Polytechnic, Kostanjeviska 16a, SI-5000 Nova Gorica, Slovenia,
  and Department of Physics, University of Ljubljana, SI-1000 Ljubljana, Slovenia
[44] Fysikum, Stockholm University, Box 6730, SE-113 85 Stockholm, Sweden
[45] Dipartimento di Fisica Sperimentale, Università di Torino and INFN, Via P. Giuria 1, IT-10125 Turin, Italy
[46] Dipartimento di Fisica, Università di Trieste and INFN, Via A. Valerio 2, IT-34127 Trieste, Italy
  and Istituto di Fisica, Università di Udine, IT-33100 Udine, Italy
[47] Univ. Federal do Rio de Janeiro, C.P. 68528 Cidade Univ., Ilha do Fundão BR-21945-970 Rio de Janeiro, Brazil
[48] Department of Radiation Sciences, University of Uppsala, P.O. Box 535, SE-751 21 Uppsala, Sweden
[49] IFIC, Valencia-CSIC, and D.F.A.M.N., U. de Valencia, Avda. Dr. Moliner 50, ES-46100 Burjassot (Valencia), Spain
[50] Institut für Hochenergiephysik, Österr. Akad. d. Wissensch., Nikolsdorfergasse 18, AT-1050 Vienna, Austria
[51] Inst. Nuclear Studies and University of Warsaw, Ul. Hoza 69, PL-00681 Warsaw, Poland
[52] Fachbereich Physik, University of Wuppertal, Postfach 100 127, DE-42097 Wuppertal, Germany
[53] On leave of absence from IHEP Serpukhov
[54] Now at University of Florida

1   Introduction

The production of several orbitally excited mesons such as $f_0(980)$ and $f_2(1270)$ [1,2], $a_0^\pm(980)$ [3], $K_2^{*0}(1430)$ [4,5] and $f_2'(1525)$ [6] has been measured by DELPHI and OPAL using the large statistics accumulated by these experiments at the Z^0 peak. A significant rate of production of $L = 1$ excited mesons in the hadronization was clearly established. Orbitally and radially excited mesons in the heavy quark sector were also observed by the LEP experiments [7–13] to be produced with significant rates.

The results obtained on the production of orbitally excited mesons in the light quark sector have usually been compared with the string [14] or cluster [15] models implemented in the QCD-based Monte Carlo generators JETSET [16] and HERWIG [17] respectively. In most cases, after proper tuning of a number of adjustable parameters, a reasonable description of the experimental data was obtained, thus allowing useful information to be obtained about the nature of the fragmentation process (see, for example, [18]). However in some cases a significant disagreement with these models was observed [5]. This is not very surprising, since the underlying physics of hadronization is not fully understood and such models cannot supply sufficiently reliable guidance on possible differences in production mechanisms of different mesons and baryons or on their dependences on spin and orbital momentum dynamics. Studies of the production properties of the orbitally excited states are thus of special interest in view of the possibly different dynamics of their production.

This paper describes new DELPHI measurements of ρ^0, $f_0(980)$, $f_2(1270)$, $K_2^{*0}(1430)$[1] and $f_2'(1525)$ production in Z^0 hadronic decays at LEP1. The previous DELPHI results on the inclusive production properties of the ρ^0, $f_0(980)$ and $f_2(1270)$ mesons [1] were based on data collected in 1991 and 1992 and were obtained without the use of particle identification. The previous DELPHI results on the $K_2^{*0}(1430)$ and $f_2'(1525)$ production [5,6] were obtained using the 1994 data sample, with particle identification coming from the RICH detectors only. The present results, superseding the previous DELPHI measurements, are based on a data sample of 2 million hadronic Z^0 decays collected during 1994 and 1995 and make use of the particle identification capabilities provided by the Ring Imaging Cherenkov (RICH) detectors and by measured ionization losses dE/dx in the Time Projection Chamber (TPC).

2   Experimental Procedure

2.1   Event and particle selection

Detailed descriptions of the DELPHI detector and its performance can be found elsewhere [19,20].

The charged particle tracks were measured in the 1.2 T magnetic field by a set of tracking detectors. The average momentum resolution for charged particles in hadronic final states, $\Delta p/p$, was usually between 0.001 and 0.01, depending on which detectors were included in the track fit.

A charged particle was accepted in this analysis if its momentum, p, was greater than 140 MeV/c, its momentum error, Δp, was less than p, its polar angle with respect to the beam axis was between 25° and 155°, its measured track length in the TPC was greater than 50 cm, and its impact parameter with respect to the nominal crossing point was within 5 cm in the transverse (xy) plane and 10 cm along the beam direction (z-axis).

---

[1]Unless otherwise stated, antiparticles are implicitly included.

Hadronic events were then selected by requiring at least 5 charged particles, with total energy of the charged particles greater than 15 GeV and at least 3 GeV in each hemisphere of the event, defined with respect to the beam direction. In addition, the polar angle of the sphericity axis was required to lie between 40° and 140°.

The sample selected with the above cuts consisted of 1.13 million events. The contamination from events due to beam-gas scattering and to $\gamma\gamma$ interactions was estimated to be less than 0.1% and the background from $\tau^+\tau^-$ events less than 0.2% of the total number accepted.

After the event selection, in order to ensure a better signal-to-background ratio for the resonances in the $\pi^+\pi^-$, $K^+\pi^-$ and K^+K^- invariant mass spectra, tighter requirements were imposed on the track impact parameters with respect to the nominal crossing point: they had to be within 0.3 cm in the transverse plane and 2 cm along the beam direction. Charged particles were used only from the barrel region of the detector and were further required to have hits in the Vertex Detector. Any particle identified by the RICH was required to have a track segment in the Outer Detector.

Charged particle identification was provided by the barrel RICH detectors for particles with momentum above 700 MeV/c, while the ionization loss measured in the TPC could be used for momenta above 100 MeV/c. The corresponding identification tags were based on the combined probabilities derived from the measured average Cherenkov angle and the number of observed photons in the RICH, and from the measured dE/dx in the TPC. Tight cuts were applied to achieve the highest possible identification purity (see [21] and references therein where further details of particle identification routines can be found). The identification performance was evaluated by means of the detector simulation program DELSIM [20]. In DELSIM, about 3 million hadronic decays of the Z^0 satisfying the same selection criteria as the real data were produced using the JETSET generator [16] with the DELPHI default parameters [18] obtained before the measurements reported in this paper. Subsequent references to JETSET always mean this tuning, which is described in detail in [18]. The particles were followed through the detector, and the simulated digitizations obtained were processed with the same reconstruction programs as the experimental data. Good agreement between the data and simulation was observed.

2.2   Fit procedure and treatment of detector response

Particle identification inefficiencies, detector imperfections such as the limited geometrical acceptance and electronic inefficiencies, particle interactions in the detector material, and the different kinematical cuts imposed for charged particle and event selection, were accounted for by applying the approach first described in [1], developed in [5,22,23] and outlined in brief below.

In the present analysis, a vector $\vec{a}$ of parameters was used in the definition of the anticipated distribution function, $f(M, \vec{a})$, of the invariant mass M. The parameters $\vec{a}$ were then determined by a least squares fit of the function to the data.

The function $f(M, \vec{a})$ was composed of three parts:

$$f(M, \vec{a}) = f^S(M, \vec{a}) + f^B(M, \vec{a}) + f^R(M, \vec{a}), \tag{1}$$

corresponding to the signal, background, and reflection contributions respectively.

The signal function, $f^S(M, \vec{a})$, described the resonance signals in the corresponding invariant mass distributions. For the $\pi^+\pi^-$ mass distributions it had the form

$$f^S(M, \vec{a}) = a_1 PS_{\rho^0}(M) \cdot BW_{\rho^0}(M, a_2, a_3) \quad + a_4 PS_{f_0}(M) \cdot BW_{f_0}(M, a_5, a_6)$$
$$+ a_7 PS_{f_2}(M) \cdot BW_{f_2}(M, a_8, a_9), \qquad (2)$$

where the relativistic Breit–Wigner functions BW for the ρ^0, $f_0(980)$ and $f_2(1270)$ are multiplied by the functions $PS(M)$ to account for the distortion of the resonance Breit–Wigner shapes by phase space effects (see [1] for details.) For each of the $K^+\pi^-$ and K^+K^- mass distributions only one Breit–Wigner term, representing the $K_2^{*0}(1430)$ and $f_2'(1525)$respectively, contributed to $f^S(M, \vec{a})$.

The background term, $f^B(M, \vec{a})$, was taken to be of the form

$$f^B(M, \vec{a}) = BG_{Jetset}(M) \cdot P(M, \vec{a}), \qquad (3)$$

where $BG_{Jetset}(M)$ represented the background shape generated by JETSET (presumed to describe the gross features of the real background) and $P(M, \vec{a}) = 1 + a_{10}M + a_{11}M^2 + a_{12}M^3 + a_{13}M^4$ was a polynomial of order 4 (or sometimes of order 3) introduced to account for possible deviations of $BG_{Jetset}(M)$ from the real background. All pairs of charged particles which do not come from the resonances considered and reflections in the invariant mass spectra were included in the definition of $BG_{Jetset}(M)$. This parameterization of the background was different from the analytical form used in a previous DELPHI analysis [1,5,22,23].

The third term, $f^R(M, \vec{a})$, represented the sum of all the reflection functions (RF_i):

$$f^R(M, \vec{a}) = \sum_{i=14}^{i=n} a_i RF_i(M), \qquad (4)$$

with different numbers n of the reflection functions for each of the mass distributions under consideration. Two types of reflection function contributing to Eq. 4 were considered. Reflections of the first type arise from particle misidentification, for example when resonances in the $K^+\pi^-$ and K^+K^- systems distort the $\pi^+\pi^-$ mass spectra. Due to the efficient particle identification of the combined RICH and TPC tags and to the high identification purity provided by the tight cuts, the influence of reflections of this type was found to be much smaller than in the previous DELPHI analysis [1], which was performed without particle identification. Reflections of the second type arise from resonances and particles decaying in the same system, for example from $K_S^0 \to \pi^+\pi^-$ or $\omega \to \pi^+\pi^- X$ in the $\pi^+\pi^-$ mass spectra, or from charmed particle production. The reflections from charmed particle decays are of special importance for the tensor mesons, as discussed in section 3.

The functions $RF_i(M)$ in Eq. 4 were determined from events generated according to the JETSET model. The contributions of the reflections to the raw mass spectra defined by the function $\bar{N}_m^R(\vec{a})$ (see Eq. 5 below) were then obtained by passing these events through the detector simulation. This also took proper account of the influence of particle misidentification.

In each mass bin, m, the number of entries $\bar{N}_m(\vec{a})$ predicted by the function $f(M, \vec{a})$, representing a sum of contributions from the resonance signals, background and reflections (see [23]), is given by

$$\bar{N}_m(\vec{a}) = C_m \sum_n S_{mn}^G A_n f_n(\vec{a}), \qquad (5)$$

$$f_n(\vec{a}) = \int_{M_n}^{M_{n+1}} f(M, \vec{a})dM, \qquad (6)$$

where $G = S$, B or R, and M_n is the lower edge of the n-th histogram bin in the distribution of the variable M. The coefficients A_n characterize the detector acceptance and the losses of particles due to the selection criteria imposed, and the C_m take into account the contamination of the sample by particles from V^0 decays, wrongly associated charged particles, secondary interactions, etc. The smearing matrix S_{mn} represents the experimental resolution. The A_n, C_m and S_{mn} were estimated separately for the resonance signals, background and reflection contributions using the detector simulation program DELSIM. Due to differences in the detector performance and data processing in different running periods, the events generated by DELSIM for these periods were taken with weights corresponding to the relative number of events in the real data. The distortion of the smearing matrix by residual Bose-Einstein correlations was also accounted for by means of the procedure described in [23].

The best values for $\vec{a}$ were then determined by a least squares fit of the predictions of Eq. 5 to the measured values, N_m, by minimizing the function

$$\chi^2 = \sum_m \left(N_m - \bar{N}_m(\vec{a})\right)^2/\sigma_m^2 + \sum_i (a_i - \bar{a}_i)^2/(\Delta \bar{a}_i)^2, \tag{7}$$

where $\sigma_m^2 = N_m + \sigma^2(\bar{N}_m)$ and $\sigma(\bar{N}_m)$ is the error on $\bar{N}_m$ due to the finite statistics of the simulation used to evaluate A_n, C_m and S_{mn}. The second sum in Eq. 7 constrains some of the fitted parameters a_i to the values $\bar{a}_i \pm \Delta \bar{a}_i$ taken from external sources, such as the normalization of the reflection functions to the particle production rates taken from this and other LEP experiments, and the masses and widths taken from the PDG tables [24]. The errors obtained from the fits thus include the corresponding systematic components.

The fits were made in the mass ranges from 0.3 to 1.8 GeV/c^2 for the $\pi^+\pi^-$, from 1.1 to 2.1 GeV/c^2 for the $K^+\pi^-$ and from 1.2 to 2.2 GeV/c^2 for the K^+K^- mass spectra.

The resonance production rates were calculated as

$$\langle N \rangle = \frac{1}{Br} \frac{1}{\langle R \rangle} \int f^S(M, \vec{a}) \, dM, \tag{8}$$

where the factor $1/Br$ (with the branching ratios, Br, from [24]) takes into account the unobserved decay modes and the integration limits are the same as the fit ranges. The factor $\langle R \rangle$, which is almost independent of the mass M, takes account of the imperfection of the detector simulation when the stronger cuts on impact parameters are applied (see [1,23] for details). It is very close to unity.

3 Results

3.1 ρ^0, $f_0(980)$ and $f_2(1270)$ production

The measured raw $\pi^+\pi^-$ invariant mass distributions are shown for the individual $x_p = p(\pi^+\pi^-)/p_{beam}$ intervals in Fig. 1 together with the results of the fits. The ρ^0 and $f_0(980)$ resonance signals are clearly seen in all x_p intervals. The relatively broad $f_2(1270)$ resonance is only just visible in the $\pi^+\pi^-$ spectra for $x_p \leq 0.4$ but is clearer after subtracting the background and reflection contributions.

The contribution of reflections is also shown in Fig. 1. As discussed in the previous section, good particle identification reduces the reflection resulting from particle misidentification to a very low level. In particular, it is seen from Fig. 1 that the reflection from the $K^{*0}(892)$ under the ρ^0 signal is almost negligible (about 2–3%). This is in stark contrast with the previous DELPHI analysis of 1991 and 1992 data [1], performed without

the use of particle identification, where the $K^{*0}(892)$ reflection contribution resulted in a strong peak in the ρ^0 mass region, comparable in magnitude with the ρ^0 signal.

The dominant contribution of the reflections is due to resonances and particles decaying into the $\pi^+\pi^- X$ systems. Their influence is mainly concentrated in the low mass region. In the ρ^0 and $f_0(980)$ mass regions, the contribution of reflections is relatively small, their mass dependence is rather smooth and therefore they do not distort the resonance signals in a significant way. However this is not the case for the $f_2(1270)$ for $x_p \geq 0.2$, where the reflections from the quasi-two-body D^0 decays, such as $D^0 \rightarrow K^{*-}(892)\pi^+$, with the π^+ from the D^0 decay and π^- from K^{*-} forming the $\pi^+\pi^-$ system, give a large contribution exactly in the $f_2(1270)$ mass region. The influence of these reflections was accounted for as discussed in sect. 2.2. In addition, possible systematic uncertainties for the $f_2(1270)$ for $x_p \geq 0.2$ arising from these reflections were accounted for in the systematic errors (see sect. 3.4).

In the fits, the ρ^0, $f_0(980)$ and $f_2(1270)$ masses and the ρ^0 and $f_2(1270)$ widths were constrained by the second term in Eq. 7 using the PDG values [24]. The $f_0(980)$ width was fixed at 50 MeV/c^2. As can be seen from Fig. 1 and Table 1, the fits describe the data very well in all measured x_p intervals, apart from the lowest x_p region, where $\chi^2/ndf \approx 2$ for 44 degrees of freedom. The ρ^0, $f_0(980)$ and $f_2(1270)$ differential production cross-sections, $(1/\sigma_h) \cdot d\sigma/dx_p$, where σ_h is the total hadronic cross-section, are presented in Table 1 and Fig. 2.

Table 1: Differential ρ^0, $f_0(980)$ and $f_2(1270)$ cross-sections $(1/\sigma_h) \cdot d\sigma/dx_p$ for the indicated x_p intervals. The errors obtained from the fits and the systematic errors are combined quadratically. The corresponding values of χ^2/ndf for the fits are also given.

$x_p\ interval$	ρ^0	$f_0(980)$	$f_2(1270)$	χ^2/ndf
$0.05 - 0.1$	6.15 ± 0.72	0.84 ± 0.16	1.23 ± 0.37	$90/44$
$0.1 - 0.2$	2.16 ± 0.23	0.35 ± 0.06	0.47 ± 0.12	$48/44$
$0.2 - 0.3$	0.92 ± 0.10	0.13 ± 0.03	0.18 ± 0.05	$58/44$
$0.3 - 0.4$	0.45 ± 0.05	0.075 ± 0.017	0.10 ± 0.04	$65/44$
$0.4 - 0.6$	0.13 ± 0.02	0.029 ± 0.006	0.042 ± 0.016	$46/44$
$0.6 - 0.8$	0.027 ± 0.005	0.006 ± 0.003	0.012 ± 0.006	$47/44$
$0.8 - 1.0$	0.003 ± 0.002	$-$	$-$	$31/46$

The rather high value of χ^2/ndf in the lowest x_p region, comes mainly from a few isolated bad points and reflects difficulties in extracting resonance rates at low momenta. Partly this is due to a poor determination of the opening angle between the low momentum particles and to the fact that a significant fraction of the particle pairs is contaminated by particles from V^0 decays and secondary interactions and by wrongly associated charged particles. For $x_p \leq 0.05$, the influence of the residual Bose-Einstein correlations, whose treatment in JETSET is not perfect, becomes very important. For these reasons, no attempt was made to measure meson resonance rates below $x_p = 0.05$ and thus this analysis is restricted to $x_p \geq 0.05$.

The measured ρ^0, $f_0(980)$ and $f_2(1270)$ rates per hadronic event in the $x_p \geq 0.05$ range, obtained by integrating the x_p spectra, were determined to be

$$\langle\rho^0\rangle_{x_p \geq 0.05} = 0.692 \pm 0.034\ (fit) \tag{9}$$

$$\langle f_0(980)\rangle_{x_p \geq 0.05} = 0.104 \pm 0.009\ (fit) \tag{10}$$

$$\langle f_2(1270)\rangle_{x_p \geq 0.05} = 0.148 \pm 0.022 \ (fit), \tag{11}$$

where the errors were obtained from the fits and, as explained in section 2.2, include a systematic component. The values (9), (10) and (11) agree with the corresponding values of 0.698 ± 0.035, 0.102 ± 0.009 and 0.145 ± 0.022, obtained by fitting the overall mass spectrum in the $x_p \geq 0.05$ range.

3.2 $K_2^{*0}(1430)$ production

The measured raw $K^+\pi^-$ invariant mass distribution for $x_p \geq 0.04$ is shown in Fig. 3 together with the results of the fit. The small $K_2^{*0}(1430)$ signal is seen in the data and its contribution is well described by the fit, with $\chi^2/ndf = 39/44$. In the fit, the $K_2^{*0}(1430)$ mass and width were constrained by the second term in Eq. 7 using the PDG values [24].

As seen from Fig. 3, the overall contribution of reflections, where charmed particle decays play the dominant role, is quite large. However their mass dependence in the $K_2^{*0}(1430)$ mass region is rather smooth and so they do not significantly distort the resonance signal. Both the shape and the normalization of the reflections in the $K^+\pi^-$ mass spectrum are well reproduced by the fit. This is seen from a very good description of the sharp peak from the two-body $D^0 \to K^-\pi^+$ decay and of the broader structure centered around 1.62 GeV caused by the quasi-two-body $D^0 \to K^{*-}(892)\pi^+$, with the π^+ from the D^0 decay and K^- from K^{*-} forming the $K^-\pi^+$ system. A fit with the contribution of the D^0 reflection left free resulted in an overall D^0 production rate of 0.392 ± 0.044, consistent within errors with the present average LEP value of 0.454 ± 0.030 [24]. This strengthens our confidence in the result obtained. The $K_2^{*0}(1430)$ signal for $x_p \geq 0.04$ shown in Fig. 3 corresponds to the production rate of

$$\langle K_2^{*0}(1430)\rangle_{x_p \geq 0.04} = 0.060 \pm 0.018 \ (fit) \tag{12}$$

per hadronic event.

3.3 $f_2'(1525)$ production

The measured raw K^+K^- invariant mass distribution for $x_p \geq 0.05$, shown in Fig. 4, exhibits some structures around 1.5–1.6 and 1.6–1.75 GeV/c^2. As discussed in [6], they could be due to the $f_2'(1525)$ and $f_J(1700)$. However, the structure around 1.5–1.6 GeV/c^2 is rather complicated, indicating that other states can possibly contribute to this mass region. Thus a contribution of the relatively narrow $f_0(1500)$, the Crystal Barrel candidate for the scalar glueball [25], and of the tensor meson $f_2(1565)$, revived recently in the analysis performed by the OBELIX collaboration [26], cannot be excluded.

Fig. 4 shows that the contribution of reflections in the mass range 1.40–1.75 GeV/c^2 is quite significant, but with a mass dependence that is comfortably small. The reflections are found to be due mainly to charmed particle decays in the K^+K^-X system. However, contrary to the situation in the $K^+\pi^-$ mass spectrum discussed in the previous section, the expected $D^0 \to K^+K^-$ signal (with $\Gamma(D^0 \to K^+K^-)/\Gamma(D^0 \to K^-\pi^+) = 0.113 \pm 0.006$ [24]) is small and poorly observed in the data. The larger contribution of this signal in the fit might be due to an overestimation of the background on account of resonances (in the mass region from 1.4 GeV/c^2 to 1.8 GeV/c^2 as discussed above) which were not included in the fit.

In this situation, a precise determination of the $f_2'(1525)$ production rate is rather difficult. As seen from Fig. 4, the fit of the K^+K^- mass spectrum with the contribution of only one $f_2'(1525)$ resonance, performed in order to obtain a rough estimate of its rate,

is not quite satisfactory in the mass region between 1.45 and 1.9 GeV/c^2, although the value of $\chi^2/ndf = 59/44$ obtained for the full mass range shows that the fit is acceptable. The $f_2'(1525)$ signal for $x_p \geq 0.05$ shown in Fig. 4 corresponds to a production rate of

$$\langle f_2'(1525) \rangle_{x_p \geq 0.05} = 0.0093 \pm 0.0038 \; (\textit{fit}) \tag{13}$$

per hadronic event.

3.4 Systematic uncertainties

The systematic uncertainties were estimated in the same way as in previous DELPHI analyses [5,23] by determining the contributions arising from:

1. variations of the charged particle selections;
2. uncertainty in particle identification efficiencies;
3. treatment of residual Bose-Einstein correlations;
4. errors in the branching ratios assumed;
5. overall normalization of reflections;
6. assumption that the relative contribution of reflections in different x_p intervals, if not taken from the LEP experiments, is the same as in JETSET;
7. extrapolation procedure used for determination of the total rate from that measured in the restricted x_p range;
8. uncertainty in the resonance line-shape, background parameterization and choice of the bin size of the mass spectra and mass range used in the fit.

The contribution of the first four factors was approximately the same for all resonances. The relative systematic error from the first factor (including uncertainty in the factor $\langle R \rangle$ in Eq. 8), affecting mostly the overall normalization of the total rates, was found to be about $\pm 2\%$, significantly smaller than in previous DELPHI analyses, reflecting a better understanding of the detector. The uncertainty in particle identification efficiencies was estimated to be around $\pm 3\%$ as follows from a more detailed analysis given in [21]. This agrees with the estimate obtained from the remaining $K^{*0}(892)$ reflection contribution under the ρ^0 signal (sect. 3.1). The systematic uncertainties arising from imperfect treatment of the residual Bose-Einstein correlations in JETSET is difficult to estimate. They were evaluated as in [1] by comparing the resonance rates obtained when the treatment of Bose-Einstein correlations was included in JETSET with those obtained when they were ignored. This gave a rather small relative error of about $\pm 2\%$, because the lowest x_p region, where the residual Bose-Einstein correlations are expected to be most significant, was not used in our analysis. The errors in the branching ratios, Br, in Eq. 8 were taken from the PDG tables [24] and amounted to $\pm 2\%$ for the $f_2(1270)$, $\pm 2.4\%$ for the $K_2^{*0}(1430)$ and $\pm 3.5\%$ for the $f_2'(1525)$.

The overall normalization of reflections and their relative contributions in different x_p intervals (factors 5 and 6) were accounted for by normalizing the contributions of the different reflections to the corresponding production rates measured at this and other LEP experiments and by using the constraints in the second term in Eq. 7. Their uncertainties are thus included in the errors obtained from the fit. The relative contributions of reflections in the different x_p intervals, if not measured, were taken from JETSET. This may result in additional systematic uncertainties for the differential cross-sections. Since JETSET describes the shape of the ρ^0, $f_0(980)$ and $f_2(1270)$ momenta spectra very well (Fig. 2), the corresponding relative systematic errors are small. However, in view of the significant contribution of the reflections from the quasi-two-body D^0 decays

in the $f_2(1270)$ mass region and some difference between Monte Carlo modelling of the $\pi^+\pi^-$ mass spectrum from charmed particle decays and the DELPHI data, systematic errors of $\pm10\%$ and $\pm15\%$ were assigned to the $f_2(1270)$ rates in the $0.2 < x_p < 0.4$ and $0.4 < x_p < 0.8$ regions respectively. This gave a relative error of $\pm3\%$ for the total $f_2(1270)$ rate. No additional systematic uncertainty due to the treatment of reflections was found to be necessary for the $K_2^{*0}(1430)$. In contrast, an error of $\pm10\%$ was assigned to the $f_2'(1525)$ total rate in view of some discrepancy between the JETSET expectation and the data for the $D^0 \to K^+K^-$ decay, thus indicating possible biases in the calculated reflection contributions to the K^+K^- mass spectrum.

The overall ρ^0, $f_0(980)$, $f_2(1270)$, $K_2^{*0}(1430)$ and $f_2'(1525)$ rates in the full x_p range were obtained from (9)–(13) by normalizing the JETSET expected rates in the x_p ranges under consideration to the data measurements in the same ranges and then taking the overall rates from the corresponding JETSET predictions. Good agreement between the measured ρ^0, $f_0(980)$ and $f_2(1270)$ x_p-spectra and JETSET predictions (Fig. 2) allowed the extrapolation error to be taken as $\pm10\%$ of the difference between the extrapolated and measured values. This gave systematic errors of $\pm4\%$ for the ρ^0 and $f_0(980)$, and $\pm3\%$ for the $f_2(1270)$ total rates. Similarly, a systematic error of $\pm2\%$ was assigned to the $K_2^{*0}(1430)$ and $f_2'(1525)$ total rates, with the assumption that JETSET describes the shapes of their x_p-spectra equally well.

The last factor accounts for uncertainties in the resonance parameterizations and fits, apart from the variation of resonance masses and widths above and below their nominal values taken from the PDG tables and accounted for in the errors on the fits[2]. The influence of variations of the bin size of the mass spectra and of the mass range used in the fit on the total ρ^0, $f_0(980)$, $f_2(1270)$ and $K_2^{*0}(1430)$ rates was found to be small. Variations of the background parameterization, using different polynomials $P(M, \vec{a})$ in the background term (3), also had negligible effects on the total rates. However, the influence of these two factors was found to be more significant for the $f_2'(1525)$ and resulted in a systematic error of $\pm11\%$ for its total rate. Systematic effects in the resonance parameterization and uncertainties in the line-shape of resonances far from the pole position, gave an error of $\pm3\%$ to the ρ^0 total rate. It was increased to $\pm5\%$ in view of possible interference between the fitted resonances or resonances and background, not accounted for in our analysis. This error was increased to $\pm7\%$ for the $f_0(980)$ and $f_2(1270)$, and to $\pm10\%$ for the $K_2^{*0}(1430)$, in view of the small rates and low signal-to-background ratios for these resonances and due to a significant coupling of the $f_0(980)$ to $K\bar{K}$ below threshold. The corresponding error for the $f_2'(1525)$, including the above mentioned $\pm11\%$, was increased to $\pm20\%$ because of the rather complicated structure of the K^+K^- mass distribution in the $f_2'(1525)$ mass region.

The overall systematic uncertainties for the resonance total rates not accounted for in the errors on the fits were therefore estimated to be $\pm7.1\%$ for the ρ^0, $\pm9.1\%$ for the $f_0(980)$, $\pm9.4\%$ for the $f_2(1270)$, $\pm11.3\%$ for the $K_2^{*0}(1430)$ and $\pm23\%$ for the $f_2'(1525)$. The correctness of these estimates of the systematic uncertainties can be assessed to some extent by comparing the present and previous DELPHI results (see next section), obtained using different data samples (especially for the ρ^0, $f_0(980)$ and $f_2(1270)$) and with a different method. Such a comparison shows that the above estimates of the systematic errors are quite reasonable.

---

[2]This does not apply to the $f_0(980)$ with the width fixed at 50 MeV and for which the results are therefore model-dependent, in view of the uncertainty on its width [24].

The overall ρ^0, $f_0(980)$, $f_2(1270)$, $K_2^{*0}(1430)$ and $f_2'(1525)$ rates in the full x_p range, obtained from (9)–(13) by applying the extrapolation procedure just described, were

$$\langle \rho^0 \rangle = 1.192 \pm 0.059 \ (fit) \pm 0.085 \ (syst) \tag{14}$$

$$\langle f_0(980) \rangle = 0.164 \pm 0.015 \ (fit) \pm 0.015 \ (syst) \tag{15}$$

$$\langle f_2(1270) \rangle = 0.214 \pm 0.032 \ (fit) \pm 0.020 \ (syst) \tag{16}$$

$$\langle K_2^{*0}(1430) \rangle = 0.073 \pm 0.022 \ (fit) \pm 0.008 \ (syst) \tag{17}$$

$$\langle f_2'(1525) \rangle = 0.012 \pm 0.005 \ (fit) \pm 0.003 \ (syst), \tag{18}$$

where the second errors represent our estimates of the systematic uncertainties.

4 Discussion

The total ρ^0, $f_0(980)$ and $f_2(1270)$ rates (14–16) can be compared with the previous values of 1.21 ± 0.15, 0.140 ± 0.034 and 0.243 ± 0.062 respectively, determined by DEL-PHI [1] from the 1991 and 1992 data samples without the use of particle identification[3]. The corresponding differential cross-sections, $(1/\sigma_h) \cdot d\sigma/dx_p$ for these two data sets are also compared in Fig. 2. In general, the agreement between the old and new results, both for the total rates and for the x_p-spectra, is very satisfactory. This shows that the rather complicated procedure of accounting for the significant reflections, which was used in this paper and was most essential for the reliable determination of the ρ^0 rate in the previous DELPHI analysis [1] without the use of particle identification, was basically correct. The largest difference between the differential cross-sections in the present and previous analyses is observed for the $f_2(1270)$ at the largest x_p values. This is understandable, since the reflections from the $K_2^{*0}(1430)$ and D^0, most significant at large x_p values, were not accounted for in [1].

The DELPHI result (14) on the total ρ^0 rate agrees within errors with the value of 1.45 ± 0.21 measured by ALEPH [27]. The x_p-spectra measured by the two experiments are also consistent with each other (Fig. 2a), although the x_p-spectrum measured by ALEPH appears to be slightly harder than that measured by DELPHI. The total ρ^0 rate (14) can also be compared with the rate 2.40 ± 0.43 of their isospin partners $\rho^{\pm}$ recently measured by OPAL [3]. The ratio of the rates, $2\langle \rho^0 \rangle / \langle \rho^{\pm} \rangle = 0.99 \pm 0.20$, is close to unity, as expected.

The total $f_0(980)$ and $f_2(1270)$ rates, (15) and (16), can be compared with the OPAL values [2] of 0.141 ± 0.013 and 0.155 ± 0.021 respectively. The DELPHI and OPAL results on the $f_0(980)$ total rate agree quite well. This is also true for the $f_0(980)$ x_p-spectra (Fig. 2b). The $f_2(1270)$ x_p-spectra measured by DELPHI and OPAL agree in shape (Fig. 2c) but differ in the absolute normalization, reflecting the difference in the respective total rates of 1.3 standard deviations.

Fig. 2 presents a comparison of the ρ^0, $f_0(980)$ and $f_2(1270)$ x_p-spectra with the expectations of the tuned JETSET model. The tuning [18] was made before this measurement, but using the previous DELPHI results on the ρ^0, $f_0(980)$ and $f_2(1270)$. Since the previous and present results are very close to each other, good agreement of the tuned JETSET model with the present DELPHI data is not surprising. It is still worth noting the good description of the ρ^0, $f_0(980)$ and $f_2(1270)$ x_p shapes by JETSET. The shapes of the ρ^0, $f_0(980)$ and $f_2(1270)$ x_p-spectra for $x_p \leq 0.4$ appear to be approximately the same. For $x_p > 0.4$, there is some indication that the $f_0(980)$ and especially the $f_2(1270)$ x_p-spectra

---

[3] These rates are obtained from the values measured in the restricted x_p ranges [1] using the same extrapolation procedure as in the present paper.

are harder than the ρ^0 x_p-spectrum. This is seen from Fig. 5, where the ratios $f_0(980)/\rho^0$ and $f_2(1270)/\rho^0$ are shown as a function of x_p. The observed increase of these ratios with x_p is consistent with the JETSET expectations.

The total $K_2^{*0}(1430)$ production rate (17) agrees, within errors, with our previous result of 0.079 ± 0.040 [5], obtained on a smaller data sample and with particle identification by the RICH only. It is also in good agreement with the DELPHI estimate of the $K_2^{*\pm}(1430)$ production rate of $0.05^{+0.07}_{-0.05}$ [1]. However the total $K_2^{*0}(1430)$ production rate (17) differs by 1.8 standard deviations from the corresponding OPAL value of 0.238 ± 0.088, obtained by extrapolation of the rate of 0.19 ± 0.07 for $x_E \leq 0.3$ measured by OPAL [4] to the full x_E range.

The total $f_2'(1525)$ production rate (18) can be compared with the previous DELPHI result of 0.020 ± 0.008 [6], again obtained from a smaller data sample and when only RICH detectors were used for particle identification. The $f_2'(1525)$ rate was also measured in [6] assuming a branching ratio $\mathrm{Br}(f_2'(1525) \rightarrow K^+ K^-) = 35.6\%$, compared with the value of 44.4% [24] in the present analysis. The values for the total $K_2^{*0}(1430)$ and $f_2'(1525)$ rates predicted by the tuned JETSET model, 0.168 and 0.024 respectively, are twice the size of those measured.

It is interesting to compare the total production rates (16), (17) and (18) of the tensor mesons $f_2(1270)$, $K_2^{*0}(1430)$ and $f_2'(1525)$ with the respective rates of the vector mesons ρ^0, $K^{*0}(892)$ and ϕ. For the ρ^0, the value (14) was used. The $K^{*0}(892)$ and ϕ total rates were taken from [5]. This gives:

$$f_2(1270)/\rho^0 = 0.180 \pm 0.035 \tag{19}$$

$$K_2^{*0}(1430)/K^{*0}(892) = 0.095 \pm 0.031 \tag{20}$$

$$f_2'(1525)/\phi = 0.115 \pm 0.058. \tag{21}$$

The $K_2^{*0}(1430)/K^{*0}(892)$ and $f_2'(1525)/\phi$ ratios are similar within large errors, but smaller than the $f_2(1270)/\rho^0$ ratio by 1.8 and 1.0 standard deviations respectively. Although the observed differences between the $K_2^{*0}(1430)/K^{*0}(892)$, $f_2'(1525)/\phi$ and $f_2(1270)/\rho^0$ ratios are not very significant, they might indicate, as has been suggested in [28], that this is a simple consequence of the difference in particle masses and the mass dependence of the production rates.

This suggestion is supported by Fig. 6, where the total rates, $\langle N(part) \rangle$, measured by DELPHI for the ρ^0, $K^{*0}(892)$, $f_0(980)$, ϕ, $f_2(1270)$, $K_2^{*0}(1430)$ and $f_2'(1525)$ are plotted as a function of their mass squared, M^2. Antiparticles are not included in the $K^{*0}(892)$ and $K_2^{*0}(1430)$ rates. Both the ρ^0, $K^{*0}(892)$, $f_0(980)$ and ϕ data points and the $f_2(1270)$, $K_2^{*0}(1430)$ and $f_2'(1525)$ data points are well described $(\chi^2/ndf = 0.07/2$ and $0.01/1)$ by exponentials of the form Ae^{-BM^2} (dashed lines in Fig. 6), with the respective slope parameters 5.43 ± 0.25 and 4.13 ± 0.63. The slopes are consistent with each other within two standard deviations. It can be noted that the ω, $\rho^\pm/2$, $a_0^\pm(980)/2$ and η' production rates measured by other LEP experiments (see [3] and references therein) are also consistent with the exponential describing the ρ^0, $K^{*0}(892)$, $f_0(980)$ and ϕ data points. Thus it appears, as already noted in [29], that the production rates of particles with similar masses, such as the ρ^0 and ω or the $f_0(980)$, $a_0^\pm(980)$ and η' are very similar.

Fig. 6 also shows that the mass dependence of the production rates is almost the same for the pairs ρ^0 and $f_2(1270)$, $K^{*0}(892)$ and $K_2^{*0}(1430)$, ϕ and $f_2'(1525)$. These three sets of data points are well fitted $(\chi^2/ndf = 0.5/2)$ to the exponential Ae^{-BM^2} (full lines in Fig. 6), with three different normalization parameters A but the *same* slope parameter B, with a fitted value of 1.74 ± 0.15. Thus the relation between the production rates of

tensor and vector mesons indeed appears to be very similar for different particles if the mass dependence of these production rates is taken into account.

The comparison of the $f_0(980)$ production rate with those of other mesons should be treated with some caution, since the results for the $f_0(980)$ are model-dependent, to a certain extent, due to the uncertainty on the $f_0(980)$ width. If the $f_0(980)$ is a conventional $q\bar{q}$ meson in the lowest $1\ ^3P_0$ multiplet with $J^{PC} = 0^{++}$ and its mixing isosinglet partner is the $f_0(1370)$, then in analogy with the tensor-to-vector meson ratios, the production rate of the $f_0(980)$ should presumably be compared with the production rate of the $\omega(1600)$, the member of the $1\ ^3D_1$ multiplet with $J^{PC} = 1^{--}$. However, the inclusive production rate of the $\omega(1600)$ is not known. The ratio of the rates of the $a_0^{\pm}(980)$ recently measured by OPAL [3] and the $f_0(980)$ (15) is 1.64 ± 0.69, compatible with a value of 2, in analogy with the $\rho^{\pm}(770)/\omega(782)$ ratio.

The total production rates of the tensor mesons $f_2(1270)$, $K_2^{*0}(1430)$ and $f_2'(1525)$ are found to be rather small in absolute value, when compared with the vector meson production rates. This agrees, at first sight, with common expectations that the production of orbitally excited states is suppressed. However, recently it was noticed [30] that the production rates of orbitally excited mesons are not smaller, but much larger relative to the states with no orbital momentum if compared *at the same masses* with the universal mass dependence of the production rates for the pseudoscalar and vector mesons and the octet and decuplet baryons [29].

Another indication for the excess of orbitally excited mesons can be seen from Table 2, where a comparison of the data with the recently proposed thermodynamical model [31] is presented. This model provides a very good description of the total production rates for the pseudoscalar and vector mesons and for the octet and decuplet baryons, both for e^+e^- [31] and for pp and $\bar{p}p$ [32] collisions. This is illustrated in Table 2 by a very good agreement between the model prediction and the data for the ρ^0. However, comparison of the model predictions with the present DELPHI results for the total production rates of orbitally excited mesons indicates that the model underestimates their yields by about the same factor of 1.6–2.1, except for the $f_2'(1525)$, where the experimental uncertainties are quite large.

Table 2: Comparison of the measured ρ^0, $f_0(980)$, $f_2(1270)$, $K_2^{*0}(1430)$ and $f_2'(1525)$ total production rates with the predictions of the thermodynamical model [31].

Particle	DELPHI results	Model predictions
ρ^0	1.19 ± 0.10	1.17 ± 0.05
$f_0(980)$	0.164 ± 0.021	0.0772 ± 0.0076
$f_2(1270)$	0.214 ± 0.038	0.130 ± 0.015
$K_2^{*0}(1430)$	0.073 ± 0.023	0.0462 ± 0.0041
$f_2'(1525)$	0.012 ± 0.006	0.0107 ± 0.0007

As suggested in [30], the large excess of orbitally excited mesons might be related to their gluonic excitation, since this can introduce angular momentum and therefore the states resulting from quarkonium-gluonium mixing might be produced at higher rates.

5 Summary

The DELPHI results on inclusive production of the ρ^0, $f_0(980)$, $f_2(1270)$, $K_2^{*0}(1430)$ and $f_2'(1525)$ in hadronic Z^0 decays at LEP have been presented. They are based on a data sample of about 2 million hadronic events, using the particle identification capabilities of the RICH and TPC detectors, and supersede the previous DELPHI results, with which they are consistent. The following conclusions can be drawn.

- The total ρ^0 production rate per hadronic Z^0 decay amounts to 1.19 ± 0.10. The ρ^0 momentum spectrum is well reproduced by the JETSET model tuned to previous DELPHI data. The total ρ^0 rate and its momentum spectrum are consistent with the ALEPH measurements.

- The total $f_0(980)$ and $f_2(1270)$ production rates per hadronic Z^0 decay are 0.164 ± 0.021 and 0.214 ± 0.038 respectively. The $f_0(980)$ and $f_2(1270)$ momentum spectra are well described by the tuned JETSET model. The shapes of the $f_0(980)$ and $f_2(1270)$ momentum spectra are similar to that for the ρ^0 for $x_p \leq 0.4$. For higher x_p values there is some indication that the ratios $f_0(980)/\rho^0$ and especially $f_2(1270)/\rho^0$ may increase with x_p, in agreement with JETSET expectations. The total $f_0(980)$ and $f_2(1270)$ rates and their momentum spectra are consistent with the OPAL measurements.

- The total $K_2^{*0}(1430)$ and $f_2'(1525)$ production rates per hadronic Z^0 decay amount to 0.073 ± 0.023 and 0.012 ± 0.006 and are about half the size of the rates predicted by the tuned JETSET model. The total $K_2^{*0}(1430)$ rate is smaller by 1.8 standard deviations than the value 0.238 ± 0.088 measured by OPAL for $x_E \leq 0.3$ and extrapolated by us to the full x_E range.

- The ratios $f_2(1270)/\rho^0$, $K_2^{*0}(1430)/K^{*0}(892)$ and $f_2'(1525)/\phi$ are 0.180 ± 0.035, 0.095 ± 0.031 and 0.115 ± 0.058 respectively. They appear to be somewhat different. However, the relationships between the production rates of the tensor and vector mesons for the $f_2(1270)$ and ρ^0, $K_2^{*0}(1430)$ and $K^{*0}(892)$, $f_2'(1525)$ and ϕ are found to be very similar when the mass dependence of the production rates is accounted for.

The DELPHI and OPAL results, despite some inconsistency between their measurements of the $K_2^{*0}(1430)$ rate, show a rather significant production rate for orbitally excited states in Z^0 hadronic decays. It appears, in agreement with the conclusions drawn in [30], that the production rates of orbitally excited tensor mesons are at least as large as those of states with no orbital momentum, if the mass dependence of their production rates is accounted for. It is also indicated that the measured rates of orbitally excited mesons are higher than follows from the thermodynamical model [31], which is quite successful in describing the total production rates of other particles.

Acknowledgements

References

[1] DELPHI Collab., P. Abreu et al., Z. Phys. **C65** (1995) 587.

[2] OPAL Collab., K. Ackerstaff et al., E. Phys. J. **C4** (1998) 19.

[3] OPAL Collab., K. Ackerstaff et al., E. Phys. J. **C5** (1998) 411.

[4] OPAL Collab., R. Akers et al., Z. Phys. **C68** (1995) 1.

[5] DELPHI Collab., P. Abreu et al., Z. Phys. **C73** (1996) 61.

[6] DELPHI Collab., P. Abreu et al., Phys. Lett. **B379** (1996) 309.

[7] ALEPH Collab., D. Buskulic et al., Z. Phys. **C73** (1997) 601.

[8] OPAL Collab., K. Ackerstaff et al., Z. Phys. **C76** (1997) 425.

[9] DELPHI Collab., P. Abreu et al., Z. Phys. **C71** (1996) 539.

[10] DELPHI Collab., P. Abreu et al., Phys. Lett. **B426** (1998) 231.

[11] DELPHI Collab., P. Abreu et al., Phys. Lett. **B345** (1995) 598.

[12] OPAL Collab., R. Akers et al., Z. Phys. **C66** (1995) 19.

[13] ALEPH Collab., D. Buskulic et al., Z. Phys. **C69** (1996) 393.

[14] B. Andersson et al., Phys. Rep. **97** (1993) 31.

[15] B.R. Webber, Nucl. Phys. **B238** (1984) 492.

[16] T. Sjöstrand, Comp. Phys. Comm. **82** (1994) 74.

[17] G. Marchesini et al., Comp. Phys. Comm. **67** (1992) 465.

[18] DELPHI Collab., P. Abreu et al., Z. Phys. **C73** (1996) 11.

[19] DELPHI Collab., P. Aarnio et al., Nucl. Instr. Meth. **A303** (1991) 233.

[20] DELPHI Collab., P. Abreu et al., Nucl. Instr. Meth. **A378** (1996) 57.

[21] DELPHI Collab., P. Abreu et al., E. Phys. J. **C5** (1998) 585.

[22] DELPHI Collab., P. Abreu et al., Phys. Lett. **B361** (1995) 207.

[23] DELPHI Collab., P. Abreu et al., Phys. Lett. **B406** (1997) 271.

[24] PDG Group, C. Caso et al., E. Phys. J. **C3** (1998) 1.

[25] Crystal Barrel Collab., V.V. Anisovich et al., Phys. Lett. **B323** (1994) 23;
A. Abele et al., Nucl. Phys. **B609** (1996) 295.

[26] OBELIX Collab., A. Bertin et al., Phys. Lett. **B408** (1997) 476.

[27] ALEPH Collab., D. Buskulic et al., Z. Phys. **C69** (1996) 379.

[28] P.V. Chliapnikov, Proceed. of the XXVI Intern. Symposium on Multiparticle Dynamics, p. 315, Faro, Portugal, 1996, Eds. J. Dias de Deus et al., World Scientific, Singapore;
V.A. Uvarov, *Experimental Studies of Hadronic Z^0 Decays with the DELPHI Detector at LEP and Searches for Regularities in Particle Production in e^+e^- Annihilations and Hadronic Collisions*, Dissertation of Doctor of Science, IHEP 98-47, Protvino, 1998.

[29] P.V. Chliapnikov and V.A. Uvarov, Phys. Lett. **B345** (1995) 313.

[30] P.V. Chliapnikov and V.A. Uvarov, Phys. Lett. **B423** (1998) 401.

[31] F. Becattini, Z. Phys. **C69** (1996) 485 and private communication.

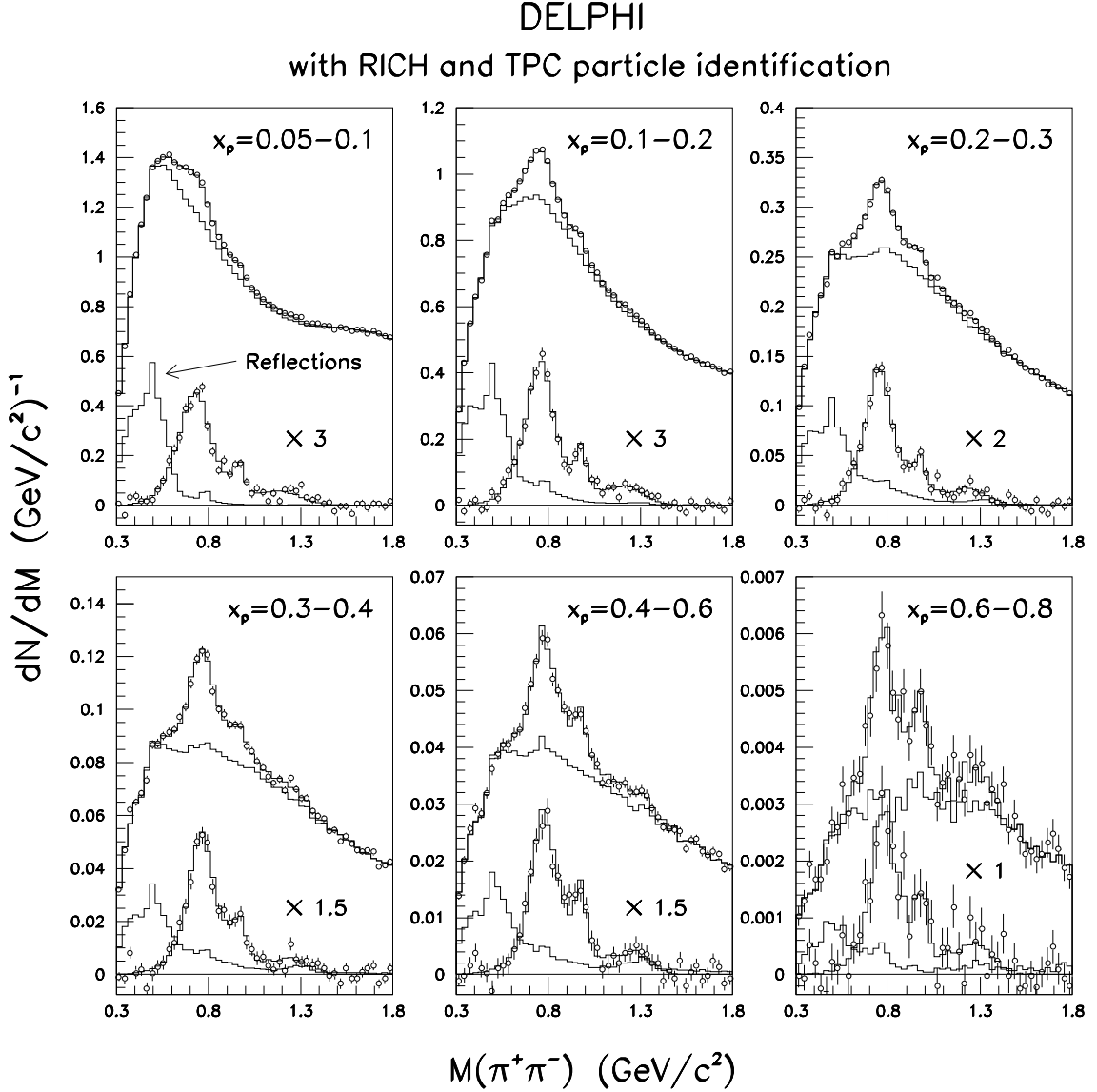[32] F. Becattini and U. Heinz, Z. Phys. **C76** (1997) 269.

Figure 1: The $\pi^+\pi^-$ invariant mass spectra for various x_p ranges as indicated. Each plot consists of an *upper* and *lower* part. In the *upper* part: the raw data are given by the open points; the upper histogram is the result of the fit; the lower histogram is the sum of the background and reflection contributions. In the *lower* part: the open points represent the data after subtraction of the background and reflections; the histograms show the contribution of reflections and result of the fit for the ρ^0, $f_0(980)$ and $f_2(1270)$ contributions. The histograms in the lower part are multiplied by the factor indicated.
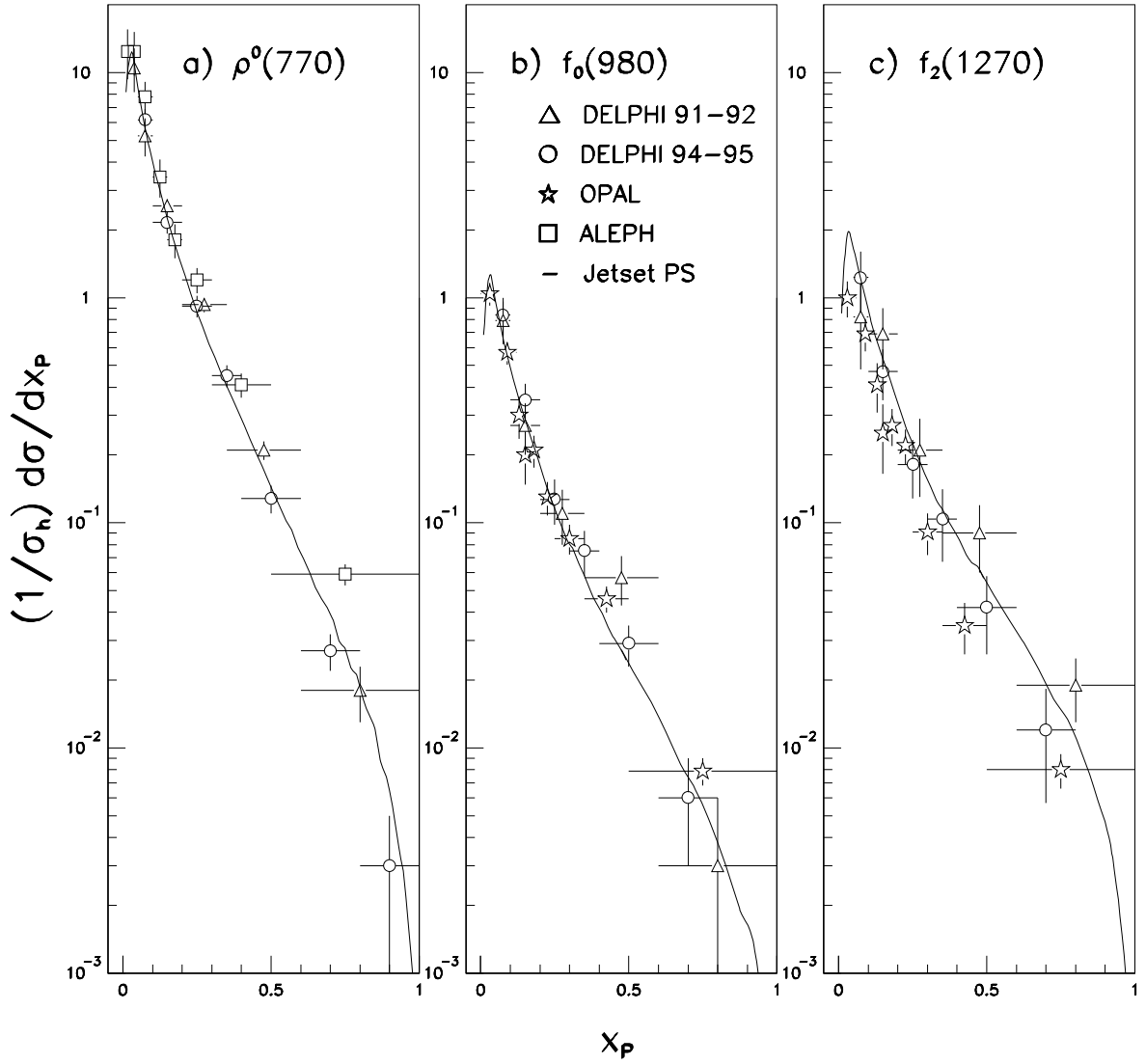
Figure 2: Differential cross-sections $(1/\sigma_h)d\sigma/dx_p$ for inclusive **a)** ρ^0, **b)** $f_0(980)$ and **c)** $f_2(1270)$ production, obtained with the 1994–1995 data (*open points*), in comparison with the previous DELPHI results based on 1991–1992 data (*triangles*), ALEPH results for the ρ^0 (*squares*) and OPAL results for the $f_0(980)$ and $f_2(1270)$ (*stars*). The *curves* represent the expectations of the tuned JETSET model.
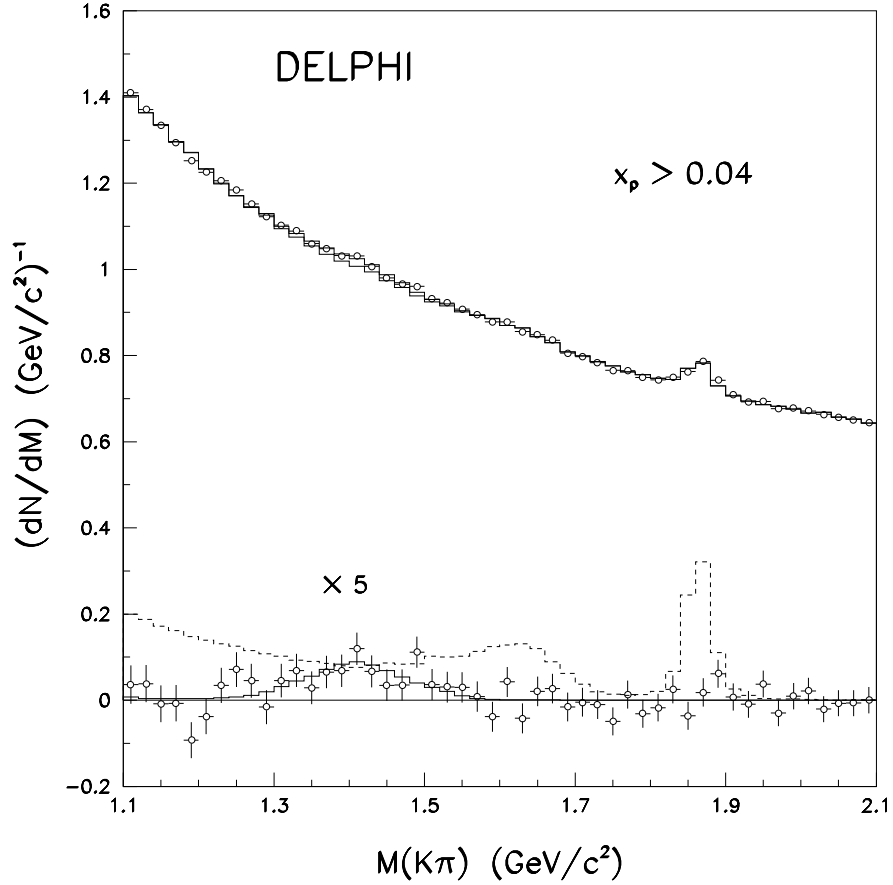
Figure 3: The $K^+\pi^-$ invariant mass spectrum for $x_p \geq 0.04$. In the *upper* part: the raw data are given by the open points; the upper histogram is the result of the fit; the lower histogram is the sum of the background and reflection contributions. In the *lower* part: the open points represent the data after subtraction of the background and reflections; the full histogram is the result of the fit for the $K_2^{*0}(1430)$ contribution; the dashed histogram shows the contribution of reflections. The histograms in the lower part are multiplied by a factor of 5.
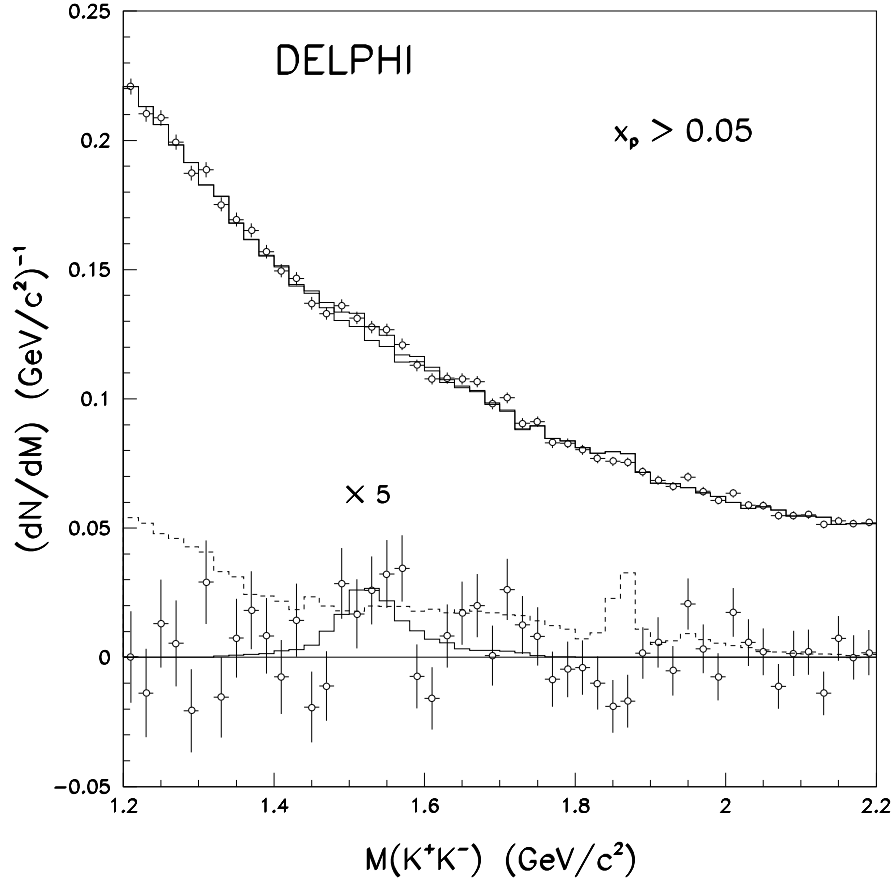
Figure 4: The K^+K^- invariant mass spectrum for $x_p \geq 0.05$. In the *upper* part: the raw data are given by the open points; the upper histogram is the result of the fit; the lower histogram is the sum of the background and reflection contributions. In the *lower* part: the open points represent the data after subtraction of the background and reflections; the full histogram is the result of the fit for the $f'_2(1525)$ contribution; the dashed histogram shows the contribution of reflections. The histograms in the lower part are multiplied by a factor of 5.
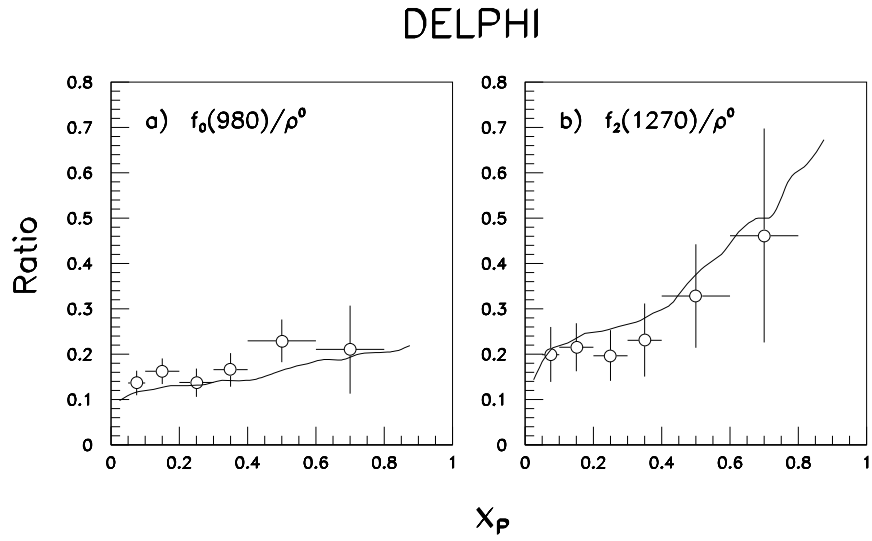
Figure 5: The ratios of the production rates **a)** $f_0(980)/\rho^0$ and **b)** $f_2(1270)/\rho^0$ as a function of x_p. The *curves* represent the expectations of the tuned JETSET model.
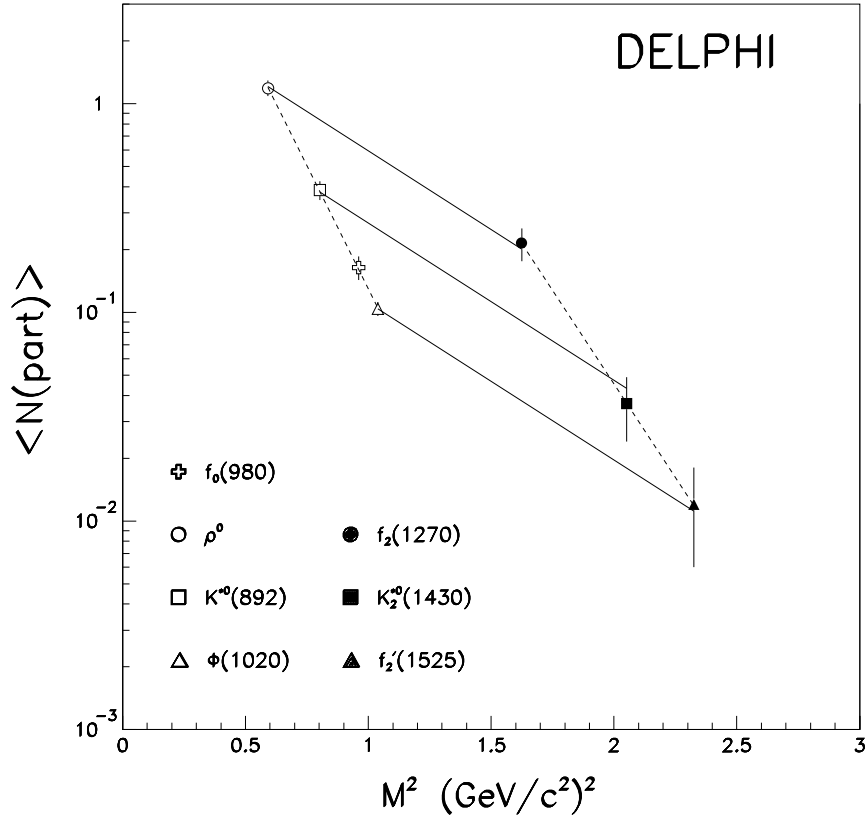
Figure 6: The production rates of the scalar, vector and tensor mesons measured by DELPHI as a function of their mass squared. The *dashed lines* represent the results of separate fits to exponentials of the ρ^0, $K^{*0}(892)$, $f_0(980)$ and ϕ rates and the $f_2(1270)$, $K_2^{*0}(1430)$ and $f_2'(1525)$ rates. The *full lines* represent the results of separate fits to three exponentials with the *same* slope of the ρ^0 and $f_2(1270)$, the $K^{*0}(892)$ and $K_2^{*0}(1430)$ rates and of the ϕ and $f_2'(1525)$ rates . The results of the fits are described in the text.